Bio-Design and Manufacturing (2024) 7:972–982
https://doi.org/10.1007/s42242-024-00308-z

RESEARCH ARTICLE

Integrated nanoporous electroporation and sensing electrode array for total dynamic time-domain cardiomyocyte membrane resealing assessment

Weiqin Sheng[1] · Ying Li[2] · Chunlian Qin[3] · Zhonghai Zhang[1] · Yuxiang Pan[3] · Zhicheng Tong[4] · Chong Teng[4] · Xinwei Wei[5]

Received: 12 August 2023 / Accepted: 14 June 2024 / Published online: 20 August 2024

Abstract

Intracellular electrophysiological research is vital for biological and medical research. Traditional planar microelectrode arrays (MEAs) have disadvantages in recording intracellular action potentials due to the loose cell–electrode interface. To investigate intracellular electrophysiological signals with high sensitivity, electroporation was used to obtain intracellular recordings. In this study, a biosensing system based on a nanoporous electrode array (NPEA) integrating electrical perforation and signal acquisition was established to dynamically and sensitively record the intracellular potential of cardiomyocytes over a long period of time. Moreover, nanoporous electrodes can induce the protrusion of cell membranes and enhance cell–electrode interfacial coupling, thereby facilitating effective electroporation. Electrophysiological signals over the entire recording process can be quantitatively and segmentally analyzed according to the signal changes, which can equivalently reflect the dynamic evolution of the electroporated cardiomyocyte membrane. We believe that the low-cost and high-performance nanoporous biosensing platform suggested in this study can dynamically record intracellular action potential, evaluate cardiomyocyte electroporation, and provide a new strategy for investigating cardiology pharmacological science.

Graphic abstract

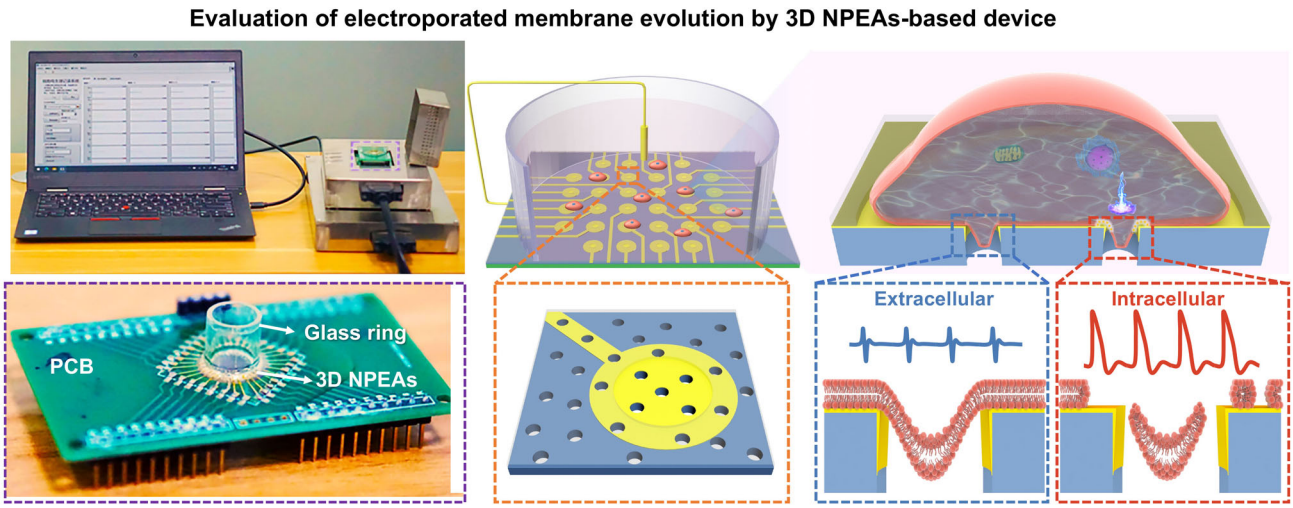

Keywords Nanoporous electrode array (NPEA) · Electroporation · Intracellular potential recording · Cardiomyocyte · Membrane resealing

Weiqin Sheng, Ying Li, and Chunlian Qin have contributed equally to this work.

Extended author information available on the last page of the article

Introduction

Regardless of the numerous breakthroughs and progress that have been made in the biomedical field, cardiovascular diseases (CVDs) remain the leading cause of mortality worldwide, accounting for approximately 30% of all deaths [1–7]. Among CVDs, cardiac arrhythmia, which is characterized by irregular electrocardiogram (ECG) and abnormal contraction of the heart, can impose a heavy burden on the heart and even cause sudden death [8–13]. Transmembrane potential analysis, which is closely related to the membrane integrity of cardiomyocytes, is important for exploring the mechanism of cardiac arrhythmias and treatment of CVDs. Currently, many research models, including cell-level action potential and ECG of ex vivo tissues or in vivo large animals, have been reported. Among these models, ECG is considered a suitable in vivo model to study cardiac arrhythmias because of its similarity to human ECG. However, it remains inapplicable for early and extensive investigation because of its low throughput, high cost, roughness, and low-resolution information, which make it unsuitable for in-depth mechanism research [14–19]. Patch clamp, a gold-standard accurate technology for electrophysiological detection, can accurately measure transmembrane potentials; however, its low throughput, severe invasiveness, and complex operation restrict the long-term recordings of multiple single cells [20–25]. Voltage-sensitive dyes have high sensitivity and resolution; however, they suffer from phototoxicity and reagent cytotoxicity, making long-term monitoring difficult [26–31]. Recently, extracellular recording microelectrodes have been proposed and widely used to perform action potential recordings in cardiomyocytes because of their non-invasive, dynamic, and large-scale characteristics. However, the loose cell–electrode interface coupling and membrane barrier lead to weak signal intensity and mismatch the native transmembrane potential [32]. Recent advances in three-dimensional (3D) microelectrodes have demonstrated that geometrical structures enhance the interface coupling of membranes and access premium intracellular recordings [33–39]. Furthermore, to perform high-quality intracellular recording, the use of appropriate assisted technology is important. Among the assisted techniques for intracellular recordings, electroporation has been widely used because it is convenient and biosafe [40–44]. During the past decades, although many efforts have been devoted to electroporation mechanism research [42, 45–50], they remain insufficient to elucidate the process of membrane perforation and resealing, attributing to the lack of a quantitative and dynamic research platform. Therefore, the development of a noninvasive, dynamic, long-term recording device for membrane evolution and intracellular action potential is crucial for the study of cardiac mechanisms and the screening of arrhythmia drugs [51–54].

In this study, a nanoporous electrode array (NPEA)-based device (Fig. 1) was suggested for dynamic evaluation of electroporated membrane evolution in cardiomyocytes and for achieving intracellular recording in a minimally invasive, long-term, and highly sensitive manner. Cell membrane evolution can also be quantitatively and segmentally studied in situ during the whole recording process (nanocrack perforation, stabilization with partial recovery, and gradual resealing) [55]. Compared with planar electrodes, 3D porous electrodes can trap and tightly couple with cultured cardiomyocytes to enhance electroporation, providing a new platform for long-term intracellular recording in the fields of cardiology and pharmacological science.

Experimental methods

Materials and reagents

Polyethylene glycol terephthalate (PET) membrane (Wuhan Kejin Xinfa Technology, China), S1813 photoresist (Rohm & Haas, USA), SU-8 2005, 2-acetoxy-1-methoxypropane (PGMEA) (Kayaku Advanced Materials, USA), quartz glass, polydimethylsiloxane 184 (PDMS 184) (Dow Corning, USA), conductive silver glue paste (Electrolube, Ashby de la Zouch, UK), 1-d-old Sprague–Dawley rats (Laboratory Animal Center of Zhejiang University, China), Dulbecco's modified Eagle medium (DMEM), Hank's balanced salt solution (HBSS), trypsin, type II collagenase, fetal bovine serum (FBS), L-glutamine, penicillin, streptomycin (Thermo Fisher Scientific, USA), and cell sieve (Sigma) were used without any further purification.

Fabrication and characterization of the nanoporous electrode array

An NPEA was fabricated on a 2 cm × 2 cm porous PET membrane with certain diameters using standard microfabrication techniques, photolithography, and magnetron sputtering according to the work of Xu et al. [56]. Typical fabrication procedures are as follows: First, the S1813 photoresist (2-μm-thick) was spined onto the porous PET membrane at 3500 r/min, followed by baking at 110 °C for 1 min. Second, an ultraviolet (UV) aligner (URE-2000/30L, Institute of Optoelectronic Technology, Chinese Academy of Sciences, China) was used to expose the PET substrate above 130 mJ/cm^2, followed by development in MF-319 (Rohm and Haas, USA) for 40 s. Third, the 10 nm Ti/50 nm Au conductive layer was sputtered onto the substrate and then lifted off in acetone. The deposited substrate was then spin-coated again with a 5-μm SU-8 layer to insulate the leads. The effective electrode region was defined again via photolithography,

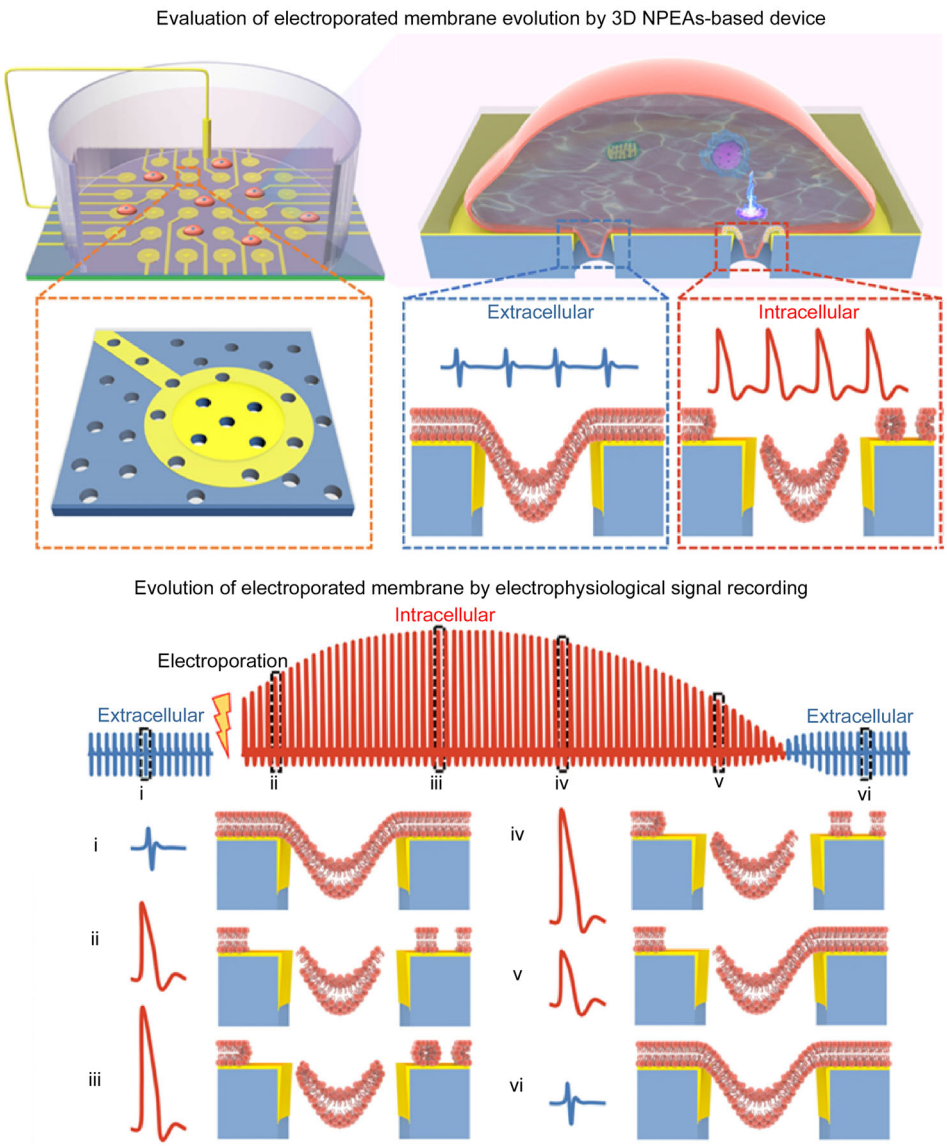

Fig. 1 Schematic of the NPEA-based sensing device for the dynamic evaluation of electroporated membrane resealing in cardiomyocytes. This integrated electroporating and sensing system can dynamically detect and analyze both extracellular and intracellular signals in real time. After electroporation, electrophysiological signals are converted from extracellular signals to intracellular signals. The amplitude quickly rises, then gradually declines, and finally returns to the extracellular state. NPEA: nanoporous electrode array

160 mJ/cm^2 exposure, and then rinsed in PGMEA and isopropanol. Finally, the fabricated device was prepared after drying in N_2 and hard baking (150 °C, 30 min). The morphologies of the fabricated devices, which were sputtered with a layer of 2 nm of Au, were characterized using scanning electron microscope (SEM) SUPRA 60 (Zeiss, Germany) at a voltage of 10 kV.

Assembly of the nanoporous electrode array

The fabricated NPEA was immobilized on a customized printed circuit board (PCB) using PDMS 184 and electrically connected using conductive silver glue paste. A cell culture chamber made of a glass ring, 0.8 cm in diameter and 1 cm in height, was then glued to the middle of a chip using PDMS. The reference electrode (Pt wire) fixed to the centrifuge tube cover was electrically connected to the PCB. The device was finally completed by soldering the pin headers on the PCB. The finished device can record the electrophysiological potentials of the cultured cardiomyocytes.

Primary rat cardiomyocyte culture

Ventricle tissues from the purchased 1-d-old Sprague–Dawley rats (75% ethanol-sterilized and ice-cold DMEM-rinsed) were sliced (about 1 mm^3) in ice-cold HBSS, which contains 0.07% trypsin and 0.05% collagenase type II, for digestion at 37 °C in an incubator (5.0% CO_2). The digestion step was repeated several times within 2 h to avoid overdigestion. The isolated cells were then purified as follows: centrifugation at 1000 r/min for 5 min, suspension in DMEM

containing 10% FBS, filtering using a 70-μm cell sieve, and purification using a differential adhesion (45 min, twice). In addition, before cell seeding, the devices were first treated with 75% ethanol and UV irradiation and then modified with fibronectin (10 μg/mL) in an incubator (37 °C, 5.0% CO_2). Finally, each device was seeded with about 3×10^5 cells in 1 mL DMEM with 10% FBS, 2 mmol/L L-glutamine, 100 U/mL penicillin, and 100 μg/mL streptomycin, which was refreshed every 48 h.

Electrophysiology recording

Electrophysiological recording of cardiomyocytes was performed using our NPEA-based system, which integrates electrical perforation and signal acquisition. First, the device with cardiomyocytes was electrically connected to a module comprising a primary amplifier and pulse signal generator. Then, the module placed in the incubator was connected to another module, which comprised a filter and a secondary amplifier, outside the incubator. Finally, pulse control of electrical perforation and signal acquisition, display, and storage were performed using a computer. Extracellular and intracellular signals (20 kHz) were filtered using a 1–7.5 kHz bandpass. To electrically perforate, 20 consecutive square-wave pulses of 200 μs pulse width and 3 V amplitude were applied to the device in 1 s.

Signal processing and statistical analysis

The LabVIEW software was used to process the signals by displaying data, removing noise, and extracting electrophysiological parameters. In the program, noise removal was performed according to the "db06" wavelet basis, and the adaptive threshold was defined using the average of the top 10 peaks in this data segment. For electrophysiological action potential spikes, the peak points were determined using the LabVIEW program's peak detection function. For the extracellular cells, valley points were also determined using the peak detection function, but for the intracellular cells, the beginning points were determined using the dynamic threshold. Other characteristic points can be determined using the peaks, valleys, and beginning points, and then used for calculating electrophysiological parameters. All results and error bars are expressed as mean ± standard deviation (SD). An ordinary one-way analysis of variance (ANOVA) was performed to analyze statistical significance using Origin 2018, and significant differences were considered at $P < 0.05$.

Results and discussion

Establishment and characterization of an intracellular electrophysiological recording system

The intracellular electrophysiological recording system comprised an NPEA device and a homemade system integrated with electroporation and signal analysis functions. The NPEA was fabricated using a standard microfabrication technique (Fig. 2a). Porous PET membranes were used as the optimum substrate for NPEA chips, which are rich in native porous structures of different sizes and densities. Steps of photolithography, sputtering with 10 nm Ti/50 nm Au, and stripping with acetone were performed to define the electrodes, tracks, and pads on the PET substrate. Finally, another 5-μm SU-8 layer was patterned to define the 30-μm electrode and insulate the leads. Compared with traditional silicon-based semiconductor processing technology that relies on etching, the above steps greatly simplify the process steps of the three-dimensional chip, improve efficiency, and save costs. As shown in Figs. 2b–2d, the 2 cm × 2 cm NPEA device had 32 electrodes, and the distance between the centers of adjacent electrodes was 300 μm, which is beneficial for reducing the mutual interference between adjacent electrodes. Considering that the diameter of adherent cardiomyocytes was 10–15 μm, the nanoporous electrode (30 μm in diameter) can sufficiently adhere to a single cardiomyocyte. Conversely, many studies suggest that the nanopore structure promotes interface coupling between the cell membrane and electrode, further reducing the interface impedance and enhancing the intracellular signal [57, 58]. Meanwhile, the nanopore's edges have a significant relationship with the cell membrane's curvature, and the curvature is beneficial for the coupling of the electrode and cell, and can delay its resealing [57–60]. The resealing time of the cell membrane is closely related to the detection window of intracellular electrophysiology. Thus, it is important to study the effect of the nanopore diameter of the electrode on membrane resealing to reveal the mechanism of intracellular electrophysiological detection. As shown in Figs. 2e–2g, SEM was employed to characterize the nanopores with different diameters (220, 450, and 1000 nm), indicating that the nanopores with different diameters possess uniform, intact porous structures. Noteworthy, the number of nanopores was inversely proportional to the diameter, and overlap occurred when the number of nanopores was large, which might affect the intensity of the intracellular electrical signal.

Furthermore, to evaluate the electrophysiological recording performance of NPEA devices with different nanopore sizes, cardiomyocytes were cultured on the assembled system (Fig. 2h), which comprised an NPEA device and a homemade analyzing system. The NPEA device was assembled using

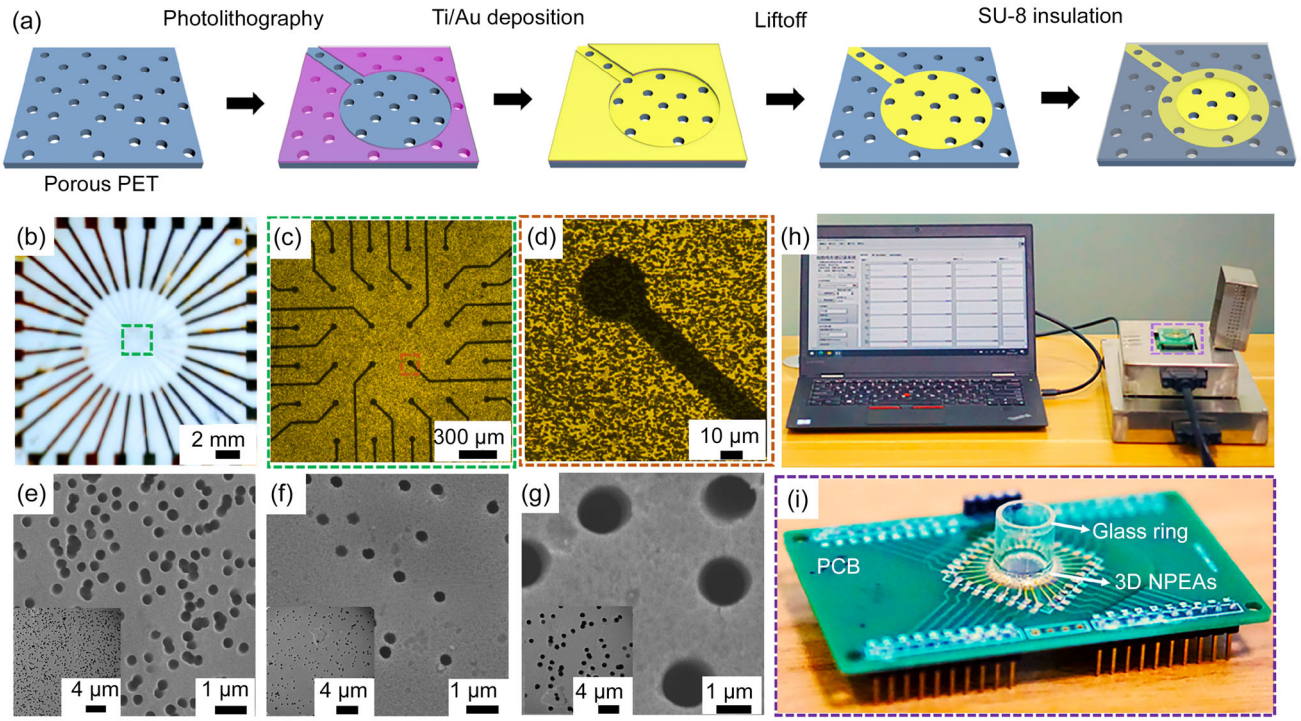

Fig. 2 Production process and characterization of 3D NPEA. **a** Flowchart for fabricating a 3D NPEA, which was patterned on a porous PET substrate according to a standard microfabrication technique. Photograph (**b**) and optical microscope images (**c**, **d**) of the 3D NPEA are shown. The distance between adjacent electrodes (the green dash box in Fig. 2b) was 300 μm, and the diameter of the working electrode (the orange dash box in Fig. 2c) was 30 μm. SEM images of nanopores with 220 nm (**e**), 450 nm (**f**), and 1000 nm (**g**) in diameter on working electrodes are shown. Insets are the corresponding SEM images of a porous working electrode site. **h** Photograph of the self-developed system for dynamic evaluation of electroporated membrane evolution in cardiomyocytes. **i** Photograph of the 3D NPEA-based device, which corresponds to the purple region in Fig. 2h. NPEA: nanoporous electrode array; PET: polyethylene glycol terephthalate; SEM: scanning electron microscope

a glass ring, a PCB base, and an NPEA chip, which was used for cardiomyocyte culturing and assessment (Fig. 2i). The homemade analyzing system is illustrated in Fig. S1 (Supplementary Information), which includes the electroporation, signal amplifying and filtering, data processing, and LabVIEW control modules. To maintain cardiomyocytes in a stable culture and assessment environment, the NPEA device was placed in a 37 °C, 5% CO_2 incubator and connected to an external laptop via a cable for long-term assessment (Fig. S2 in Supplementary Information). The homemade LabVIEW program can control electroporation, record intracellular electrical signals, and evaluate the resealing of the cardiomyocyte membrane (Fig. S3 in Supplementary Information). The corresponding SEM image of cardiomyocytes coupled to the NPEA device is also shown in Fig. S4 (Supplementary Information), indicating that cardiomyocytes with good morphology are closely diffused and bound to the NPEA device.

Total time-domain assessment of cardiomyocyte membrane resealing

Cell membrane electroporation is a technique for establishing access to intracellular electrophysiology, which introduces transient pulse voltage to lower cell–electrode interface impedance and breakdown cell membrane dielectric, inducing nanocracks on the membrane [43]. Because of the self-healing properties of the cell membrane, the nanocracks on the membrane reseal after electroporation. Additionally, ion channels on the cell membrane play an important role in transmembrane potential regulation [61]. Therefore, the assessment of membrane status is important for recording intracellular electrophysiology and studying the mechanism of ion channel drug intervention. Although conventional microelectrode arrays (MEAs) can evaluate cell membrane status by recording extracellular potential, the cell membrane barrier of the cell–electrode interface remains a hindrance. The natural barrier causes a large sealing impedance and weakens the action potential signal acquisition. In this study,

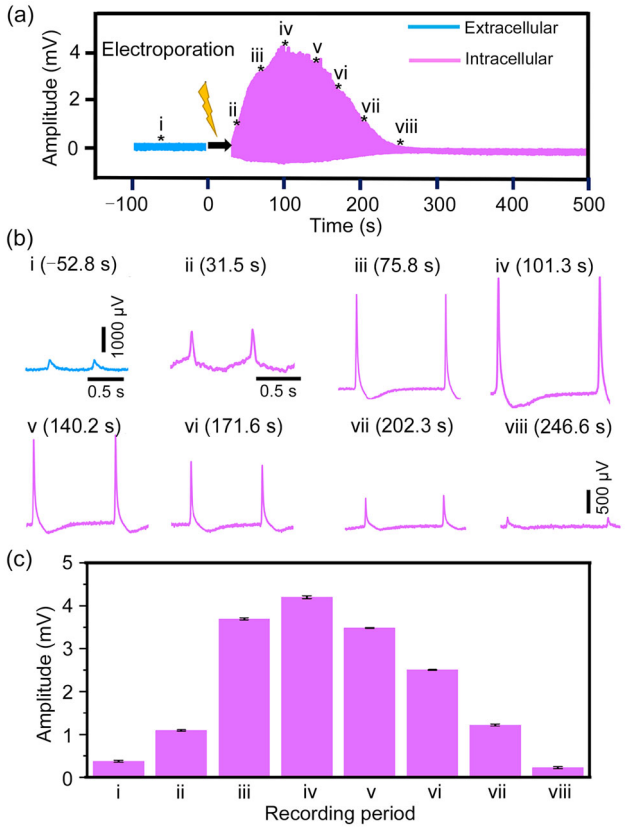

Fig. 3 Dynamic assessment of the electroporated membrane evolution in cardiomyocytes through continuous electrophysiological recordings. Typical extracellular (blue) and intracellular (rose red) recordings (**a**) and corresponding enlargements (**b**). **c** Amplitude data at different recording periods

NPEA performed electroporation and intracellular electrophysiological recordings, and cell membrane resealing was evaluated via real-time assessment of action potential.

Extracellular and intracellular action potential recordings for membrane dynamic evaluation are shown in Fig. 3a. This suggests that cardiomyocytes can first generate low-quality extracellular potentials, quickly convert them to intracellular potentials with maximum amplitude upon 3 V electroporation, and finally return to the extracellular state. The conversion between extracellular and intracellular signals demonstrated nanocrack generation and resealing on the cell membrane. From the whole recordings, the extracted signals can be analyzed in detail (Fig. 3b). The initial extracellular action potential was 375.68 μV at about −52.8 s (i) and was then converted to intracellular potential after electroporation. The intracellular action potential started from 1092.53 μV at 31.5 s (ii) to 3697.37 μV at 75.8 s (iii), quickly reached a maximum of 4197.65 μV at 101.3 s (iv), and then slowly decreased (3483.30 μV at 140.2 s (v), 2506.79 μV at 171.6 s (vi), and 1220.01 μV at 202.3 s (vii)). Finally, it returned to the extracellular state (221.84 μV at 246.6 s (viii)). The whole converting process (Figs. 3b and 3c) of the electroporated cell membrane reveals its reversibility, suggesting its potential application in evolution assessment by continuous electrophysiological recordings in a dynamic and quantitative manner. Additionally, a device with a good spatial and temporal resolution of action potential is expected to be used in the development of cardiac drugs (Fig. S5 in Supplementary Information). The drug test results showed that our porous device is sensitive to such drug screens. Furthermore, based on its high spatiotemporal resolution characteristics, this device may be used to monitor neuroelectrophysiological signals.

Optimization of intracellular electrophysiological recording using a nanoporous electrode array

To confirm the electrophysiological recording performance of NPEA, electroporated cardiomyocyte membranes were assessed in real time using MEA (planar, 2 cm × 2 cm) and NPEA (porous) (Fig. 4a). By statistically analyzing the intracellular amplitudes (Fig. 4b) and signal-to-noise ratios (SNRs) (Fig. 4c) of the nanoporous and planar electrode recordings, the average amplitude and SNR for the nanoporous electrode were 1.68 mV and 26.85 dB, respectively, which are much higher than that of the planar electrode (0.57 mV and 20.73 dB, respectively). The SNR of the extracellular raw noise levels was also plotted (Fig. S6 in Supplementary Information), indicating that the porous device is also sensitive in the extracellular cell. In addition, the amplitude and its variation in a short time before (increase stage) and after (decrease stage) electroporation were studied using different microelectrodes (Figs. 4d and 4e). The time point for electroporation was set to 0 s. Figure 4d shows that the amplitude and its variation of both 3D porous and planar electrodes increase slightly over time before electroporation, but the nanoporous electrode had a slightly higher value near the electroporation, indicating that the nanoporous electrode is more sensitive to recording than the planar electrode. Simultaneously, after electroporation, the amplitudes gradually decreased, suggesting slow resealing of the cell membrane. Conversely, the amplitude variation rates first reached a negative peak and then slowly increased to approximately 0, indicating cell membrane recovery (Fig. 4e). Additionally, the amplitude for the nanoporous electrode was higher than that for the planar electrode, suggesting a higher sensitivity of the nanoporous electrode. On the basis of the above results, NPEA showed excellent performance in dynamically recording electroporated membrane evolution.

The successful monitoring of membrane resealing demonstrated that NPEA can dynamically assess cell membrane status by recording intracellular electrophysiological signals. Research shows that nanopores on the electrode are helpful for electroporation and resealing by enhancing the

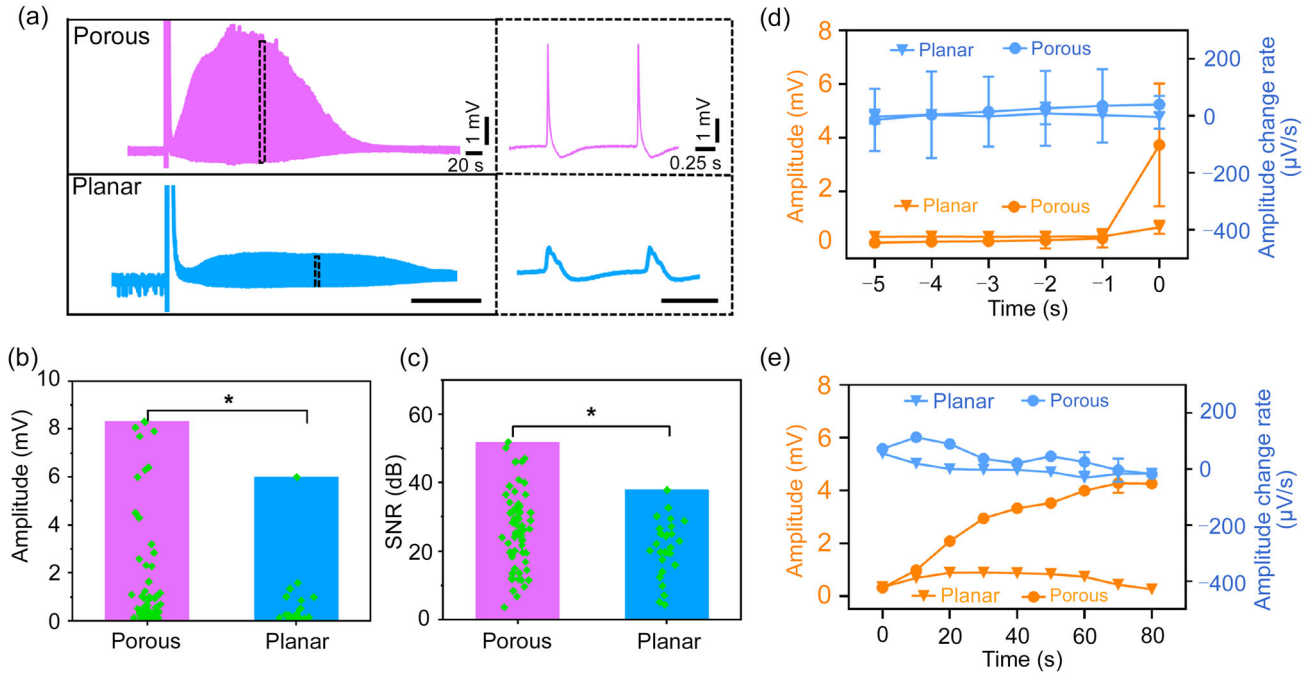

Fig. 4 **a** Electrophysiological recording using electrodes with different shapes (rose red for 3D NPEA and blue for planar MEA). Enlarged signals show the typical shape of the intracellular action potential. Statistical measurements of the intracellular amplitude (**b**) and SNR (**c**) recorded using different MEAs. An ordinary one-way ANOVA was used to analyze statistical significance, $^{*}P < 0.05$. Evolution of the amplitude (orange) and its rate of change (blue) of the action potential before (**d**) and after (**e**) electroporation. The time required to reach the maximum was set to 0 s, and the error bars are presented as mean ± SD ($n = 3$). NPEA: nanoporous electrode array; MEA: microelectrode array; SNR: signal-to-noise ratio; ANOVA: analysis of variance; SD: standard deviation

coupling between the cell membrane and electrode [57, 58, 62, 63]. The interface between the electrode and cell implies much information for intracellular recording via signal transmission and electroporation. The electric field models of the NPEA and MEA were established using COMSOL, as shown in Figs. S7–S9 (Supplementary Information). The NPEA had stronger electric field penetration, especially in the nanoporous area, which is almost five times that of MEA, and the magnitude distribution was more uniform. A possible reason for this phenomenon may be that the pore structure with broadband characteristics and low losses can be regarded as an isotropic structure, and its electromagnetic characteristics are consistent for waves in different directions. Compared with planar structures, porous structures can improve their relative dielectric constant and other electromagnetic characteristics, resulting in a more concentrated electric field intensity. As long as the number of pores with a certain diameter on the electrode is large, the electric field intensity can be sufficiently concentrated. Noteworthy, the more uniform the pore distribution, the more conducive it is to the concentration of the electric field, but the pore distribution with low uniformity also has this tendency to cause the electric field to concentrate. To further optimize the recording of electrophysiological signals, nanopores on electrodes with different diameters (220, 450, and 1000 nm) were used to record the electrophysiological potential (Fig. 5a). By statistically analyzing the intracellular potential amplitudes (Fig. 5b), SNRs (Fig. 5c), and durations (Fig. 5d) collected by the nanoporous electrodes with diameters of 220, 450, and 1000 nm, the maximum potential amplitudes were 2.83, 8.33, and 2.62 mV, the average SNR values were 18.84, 26.74, 17.28 dB, and the maximum durations were 599.74, 570.46, and 350.93 s, respectively. The results above show that the intracellular potential recorded using the 3D porous device with a 450-nm diameter has a larger percentage in high amplitude and SNR, although its duration is a little short. A possible reason for this may be the better performance of nanoporous devices with more pores and longer circumferences, which can supply more sites for cardiomyocytes to improve sealing and electroporation. However, if the pore diameter is too small, the cell membrane cannot protrude into the nanocracks, thus increasing signal loss and preventing electrodes from accessing the interior.

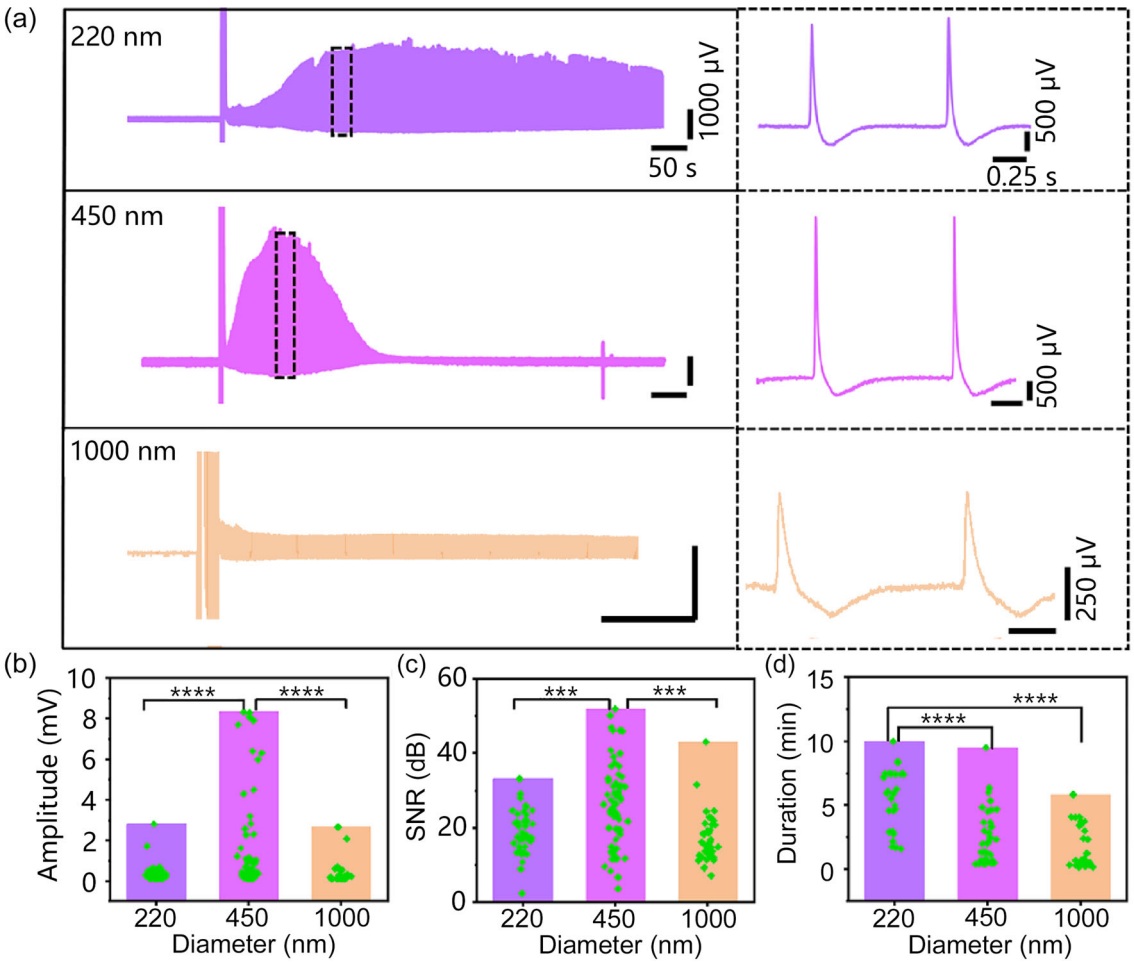

Fig. 5 **a** Electrophysiological recording using NPEA with different pore diameters. The enlarged signal shows the typical shape of the intracellular action potential. **b–d** Statistical measurements of the intracellular action potential amplitude, SNR, and duration recorded using NPEA with different diameters. An ordinary one-way ANOVA was used to analyze statistical significance. $^{***}P < 0.001$; $^{****}P < 0.0001$. NPEA: nanoporous electrode array; SNR: signal-to-noise ratio; ANOVA: analysis of variance

Conclusions

In this study, an electrophysiological sensing device based on NPEA for dynamic evaluation of electroporated membrane evolution, which can dynamically detect and analyze both extracellular and intracellular signals with high sensitivity and throughput for a long time, was developed. During the entire recording process, the signals can be analyzed quantitatively and segmentally according to their amplitudes and change rates of amplitude, which can conveniently represent cell membrane evolution. In summary, the low-cost and high-performance sensing platform suggested in this study can dynamically record the intracellular action potential and evaluate cardiomyocyte electroporation, providing a novel strategy for studying the evolution of electroperforated membranes and understanding the electroporation mechanism in depth.

However, there are still some other works that need to be done in the future, such as (i) selecting a 3D nanodevice with other nanostructures (morphology, size, material, etc.) to enhance the cell–electrode coupling and achieve an intracellular recording with long-term and high sensitivity and (ii) enlarging the application field (drug screening, intracellular delivery, etc.) of the self-developed sensing device through other models (other cell types and neuron).

Supplementary Information The online version contains supplementary material available at https://doi.org/10.1007/s42242-024-00308-z.

Acknowledgements This work was supported by the Zhejiang Provincial Natural Science Foundation of China (No. LQ23E010004) and the National Key Research and Development Program of China (No. 2021YFB3200801).

Author contributions WQS, YL, and CLQ performed all experiments and conducted data analysis. ZHZ carried out the electric field model simulation of different electrode arrays. ZCT took some data analysis

in the stage of replying to the reviewers' comments and redrew a figure. YXP, CT, and XWW revised the manuscript and provided project guidance. In particular, CT and XWW conceived the whole reply idea of this work and pointed out the direction of the reply. All authors read and approved the final manuscript.

Declarations

Conflict of interest The authors declare that they have no conflict of interest.

Ethical approval All protocols comply with the charter of the Ethical Review Committee of Laboratory Animal Welfare of Zhejiang University, China.

References

1. Feigin VL, Forouzanfar MH, Krishnamurthi R et al (2014) Global and regional burden of stroke during 1990–2010: findings from the Global Burden of Disease Study 2010. Lancet 383(9913):245–255. https://doi.org/10.1016/S0140-6736(13)61953-4
2. Vos T, Abajobir AA, Abbafati C et al (2017) Global, regional, and national incidence, prevalence, and years lived with disability for 328 diseases and injuries for 195 countries, 1990–2016: a systematic analysis for the Global Burden of Disease Study 2016. Lancet 390(10100):1211–1259. https://doi.org/10.1016/S0140-6736(17)32154-2
3. Hong J, Kim K, Kim JH et al (2017) The role of endoplasmic reticulum stress in cardiovascular disease and exercise. Int J Vasc Med 2017:2049217. https://doi.org/10.1155/2017/2049217
4. Kontis V, Mathers CD, Rehm J et al (2014) Contribution of six risk factors to achieving the 25×25 non-communicable disease mortality reduction target: a modelling study. Lancet 384(9941):427–437. https://doi.org/10.1016/S0140-6736(14)60616-4
5. Ma LY, Chen WW, Gao RL et al (2020) China cardiovascular diseases report 2018: an updated summary. J Geriatr Cardiol 17(1):1–8. https://doi.org/10.11909/j.issn.1671-5411.2020.01.001
6. Wong ND (2014) Epidemiological studies of CHD and the evolution of preventive cardiology. Nat Rev Cardiol 11(5):276–289. https://doi.org/10.1038/nrcardio.2014.26
7. Zhao YL, You SS, Zhang AQ et al (2019) Scalable ultrasmall three-dimensional nanowire transistor probes for intracellular recording. Nat Nanotechnol 14(8):783–790. https://doi.org/10.1038/s41565-019-0478-y
8. Auer R, Bauer DC, Marques-Vidal P et al (2012) Association of major and minor ECG abnormalities with coronary heart disease events. JAMA 307(14):1497–1505. https://doi.org/10.1001/jama.2012.434
9. Denes P, Larson JC, Lloyd-Jones DM et al (2007) Major and minor ECG abnormalities in asymptomatic women and risk of cardiovascular events and mortality. JAMA 297(9):978–985. https://doi.org/10.1001/jama.297.9.978
10. Hong YJ, Jeong H, Cho KW et al (2019) Wearable and implantable devices for cardiovascular healthcare: from monitoring to therapy based on flexible and stretchable electronics. Adv Funct Mater 29(19):1808247. https://doi.org/10.1002/adfm.201808247
11. Littlejohns TJ, Holliday J, Gibson LM et al (2020) The UK Biobank imaging enhancement of 100,000 participants: rationale, data collection, management and future directions. Nat Commun 11(1):2624. https://doi.org/10.1038/s41467-020-15948-9
12. McCorquodale A, Poulton R, Hendry J et al (2017) High prevalence of early repolarization in the paediatric relatives of sudden arrhythmic death syndrome victims and in normal controls. Europace 19(8):1385–1391. https://doi.org/10.1093/europace/euw248
13. Xiang ZH, Han MD, Zhang HX (2023) Nanomaterials based flexible devices for monitoring and treatment of cardiovascular diseases (CVDs). Nano Res 16(3):3939–3955. https://doi.org/10.1007/s12274-022-4551-8
14. Gintant G, Sager PT, Stockbridge N (2016) Evolution of strategies to improve preclinical cardiac safety testing. Nat Rev Drug Discov 15(7):457–471. https://doi.org/10.1038/nrd.2015.34
15. Horvath P, Aulner N, Bickle M et al (2016) Screening out irrelevant cell-based models of disease. Nat Rev Drug Discov 15(11):751–769. https://doi.org/10.1038/nrd.2016.175
16. Itzhaki I, Maizels L, Huber I et al (2011) Modelling the long QT syndrome with induced pluripotent stem cells. Nature 471(7337):225–229. https://doi.org/10.1038/nature09747
17. Mummery C, Ward-Van Oostwaard D, Doevendans P et al (2003) Differentiation of human embryonic stem cells to cardiomyocytes: role of coculture with visceral endoderm-like cells. Circulation 107(21):2733–2740. https://doi.org/10.1161/01.CIR.0000068356.38592.68
18. Ronaldson-Bouchard K, Vunjak-Novakovic G (2018) Organs-on-a-chip: a fast track for engineered human tissues in drug development. Cell Stem Cell 22(3):310–324. https://doi.org/10.1016/j.stem.2018.02.011
19. Shang YX, Chen ZY, Zhang ZH et al (2020) Heart-on-chips screening based on photonic crystals. Bio-Des Manuf 3(3):266–280. https://doi.org/10.1007/s42242-020-00073-9
20. Chen PH, Zhang W, Zhou J et al (2009) Development of planar patch clamp technology and its application in the analysis of cellular electrophysiology. Prog Nat Sci-Mater Int 19:153–160
21. Craighead H (2006) Future lab-on-a-chip technologies for interrogating individual molecules. Nature 442(7101):387–393. https://doi.org/10.1038/nature05061
22. Li XH, Klemic KG, Reed MA et al (2006) Microfluidic system for planar patch clamp electrode arrays. Nano Lett 6:815–819. https://doi.org/10.1021/nl060165r
23. Liu QJ, Wu CS, Cai H et al (2014) Cell-based biosensors and their application in biomedicine. Chem Rev 114(12):6423–6461. https://doi.org/10.1021/cr2003129
24. Li WE, Luo XJ, Ulbricht Y et al (2019) Establishment of an automated patch-clamp platform for electrophysiological and pharmacological evaluation of hiPSC-CMs. Stem Cell Res 41:101662. https://doi.org/10.1016/j.scr.2019.101662
25. Sakmann B, Neher E (1984) Patch clamp techniques for studying ionic channels in excitable membranes. Annu Rev Physiol 46(1):455–472. https://doi.org/10.1146/annurev.ph.46.030184.002323
26. Matiukas A, Mitrea BG, Qin MC et al (2007) Near-infrared voltage-sensitive fluorescent dyes optimized for optical mapping in bloodperfused myocardium. Heart Rhythm 4(11):1441–1451. https://doi.org/10.1016/j.hrthm.2007.07.012
27. Klimas A, Ambrosi CM, Yu JZ et al (2016) OptoDyCE as an automated system for high-throughput all-optical dynamic cardiac electrophysiology. Nat Commun 7(1):11542. https://doi.org/10.1038/ncomms11542
28. Sayresmith NA, Saminathan A, Sailer JK et al (2019) Photostable voltage-sensitive dyes based on simple, solvatofluorochromic, asymmetric thiazolothiazoles. J Am Chem Soc 141(47):18780–18790. https://doi.org/10.1021/jacs.9b08959
29. Hochbaum DR, Zhao YX, Farhi SL et al (2014) All-optical electrophysiology in mammalian neurons using engineered microbial rhodopsins. Nat Methods 11(8):825–833. https://doi.org/10.1038/nmeth.3000

30. Zhou YC, Liu E, Muller H et al (2021) Optical electrophysiology: toward the goal of label-free voltage imaging. J Am Chem Soc 143(28):10482–10499. https://doi.org/10.1021/jacs.1c02960
31. Xue JJ, Shao M, Gao ZG et al (2023) Advances in micro-nano biosensing platforms for intracellular electrophysiology. J Zhejiang Univ-SCI A (Appl Phys & Eng) 24(11):1017–1026. https://doi.org/10.1631/jzus.A2300267
32. Hofmann B, Katelhon E, Schottdorf M et al (2011) Nanocavity electrode array for recording from electrogenic cells. Lab Chip 11(6):1054–1058. https://doi.org/10.1039/c0lc00582g
33. Abbott J, Ye TY, Ham D et al (2018) Optimizing nanoelectrode arrays for scalable intracellular rlectrophysiology. Acc Chem Res 51(3):600–608. https://doi.org/10.1021/acs.accounts.7b00519
34. Dipalo M, Amin H, Lovato L et al (2017) Intracellular and extracellular recording of spontaneous action potentials in mammalian neurons and cardiac cells with 3D plasmonic nanoelectrodes. Nano Lett 17(6):3932–3939. https://doi.org/10.1021/acs.nanolett.7b01523
35. Jahed Z, Yang Y, Tsai CT et al (2022) Nanocrown electrodes for parallel and robust intracellular recording of cardiomyocytes. Nat Commun 13:2253. https://doi.org/10.1038/s41467-022-29726-2
36. Pei F, Tian BZ (2019) Nanoelectronics for minimally invasive cellular recordings. Adv Funct Mater 30(29):1906210. https://doi.org/10.1002/adfm.201906210
37. Spira ME, Hai A (2013) Multi-electrode array technologies for neuroscience and cardiology. Nat Nanotechnol 8(2):83–94. https://doi.org/10.1038/NNANO.2012.265
38. Zhang AQ, Lieber CM (2016) Nano-bioelectronics. Chem Rev 116(1):215–257. https://doi.org/10.1021/acs.chemrev.5b00608
39. Zhou NJ, Ma L (2022) Smart bioelectronics and biomedical devices. Bio-Des Manuf 5(1):1–5. https://doi.org/10.1007/s42242-021-00179-8
40. Dipalo M, Rastogi SK, Matino L et al (2021) Intracellular action potential recordings from cardiomyocytes by ultrafast pulsed laser irradiation of fuzzy graphene microelectrodes. Sci Adv 7(15):eabd5175. https://doi.org/10.1126/SCIADV.ABD5175
41. Kotnik T, Frey W, Sack M et al (2015) Electroporation-based applications in biotechnology. Trend Biotechnol 33(8):480–488. https://doi.org/10.1016/j.tibtech.2015.06.002
42. Kotnik T, Rems L, Tarek M et al (2019) Membrane electroporation and electropermeabilization: mechanisms and models. Annu Rev Biophys 48(1):63–91. https://doi.org/10.1146/annurev-biophys-052118-115451
43. Shokouhi AR, Aslanoglou S, Nisbet D et al (2020) Vertically configured nanostructure-mediated electroporation: a promising route for intracellular regulations and interrogations. Mater Horiz 7(11):2810–2831. https://doi.org/10.1039/d0mh01016b
44. Zhao J, Wen XF, Tian L et al (2019) Irreversible electroporation reverses resistance to immune checkpoint blockade in pancreatic cancer. Nat Commun 10(1):899. https://doi.org/10.1038/s41467-019-08782-1
45. Chu KF, Dupuy DE (2014) Thermal ablation of tumours: biological mechanisms and advances in therapy. Nat Rev Cancer 14(3):199–208. https://doi.org/10.1038/nrc3672
46. Gurtovenko AA, Vattulainen I (2005) Pore formation coupled to ion transport through lipid membranes as induced by transmembrane ionic charge imbalance: atomistic molecular dynamics study. J Am Chem Soc 127(50):17570–17571. https://doi.org/10.1021/ja053129n
47. Kanade PP, Oyunbaatar NE, Shanmugasundaram A et al (2022) MEA-integrated cantilever platform for comparison of real-time change in electrophysiology and contractility of cardiomyocytes to drugs. Biosens Bioelectron 216:114675. https://doi.org/10.1016/j.bios.2022.114675
48. Kim V, Semenov I, Kiester AS et al (2023) Action spectra and mechanisms of (in) efficiency of bipolar electric pulses at electroporation. Bioelectrochemistry 149:108319. https://doi.org/10.1016/j.bioelechem.2022.108319
49. Stewart MP, Langer R, Jensen KF (2018) Intracellular delivery by membrane disruption: mechanisms, strategies, and concepts. Chem Rev 118(16):7409–7531. https://doi.org/10.1021/acs.chemrev.7b00678
50. Tarek M (2005) Membrane electroporation: a molecular dynamics simulation. Biophys J 88(6):4045–4053. https://doi.org/10.1529/biophysj.104.050617
51. Yang Y, Liu AF, Tsai CT et al (2022) Cardiotoxicity drug screening based on whole-panel intracellular recording. Biosens Bioelectron 216:114617. https://doi.org/10.1016/j.bios.2022.114617
52. Chen HW, Zhang Y, Zhang LW et al (2021) Applications of bioinspired approaches and challenges in medical devices. Bio-Des Manuf 4(1):146–148. https://doi.org/10.1007/s42242-020-00103-6
53. Wu GH, Wu JG, Li ZH et al (2022) Development of digital organ-on-a-chip to assess hepatotoxicity and extracellular vesicle-based anti-liver cancer immunotherapy. Bio-Des Manuf 5(3):437–450. https://doi.org/10.1007/s42242-022-00188-1
54. Zhang YS, Khademhosseini A (2020) Engineering in vitro human tissue models through bio-design and manufacturing. Bio-Des Manuf 3(3):155–159. https://doi.org/10.1007/s42242-020-00080-w
55. Zhang MY, Xu DX, Fang JR et al (2022) A dynamic and quantitative biosensing assessment for electroporated membrane evolution of cardiomyocytes. Biosens Bioelectron 202:114016. https://doi.org/10.1016/j.bios.2022.114016
56. Xu DX, Xiao HB, Wang SZ et al (2022) Universal and sensitive drug assessment biosensing platform using optimal mechanical beating detection of single cardiomyocyte. ACS Nano 16(9):15484–15494. https://doi.org/10.1021/acsnano.2c08049
57. Lin ZC, Xie C, Osakada Y et al (2014) Iridium oxide nanotube electrodes for sensitive and prolonged intracellular measurement of action potentials. Nat Commun 5:3206. https://doi.org/10.1038/ncomms4206
58. Karatekin E, Sandre O, Guitouni H et al (2003) Cascades of transient pores in giant vesicles: line tension and transport. Biophys J 84(3):1734–1749. https://doi.org/10.1016/S0006-3495(03)74981-9
59. McNeil PL, Kirchhausen T (2005) An emergency response team for membrane repair. Nat Rev Mol Cell Biol 6(6):499–505. https://doi.org/10.1038/nrm1665
60. Steinhardt RA, Bi G, Alderton JM (1994) Cell membrane resealing by a vesicular mechanism similar to neurotransmitter release. Science 263(5154):390–393. https://doi.org/10.1126/science.7904084
61. Catterall WA (2000) Structure and regulation of voltage-gated Ca^{2+} channels. Annu Rev Cell Dev Biol 16(1):521–555. https://doi.org/10.1146/annurev.cellbio.16.1.521
62. Lira RB, Leomil FSC, Melo RJ et al (2021) To cose or to collapse: the role of charges on membrane stability upon pore formation. Adv Sci 8(11):2004068. https://doi.org/10.1002/advs.202004068
63. Elnathan R, Barbato MG, Guo XF et al (2022) Biointerface design for vertical nanoprobes. Nat Rev Mater 7(12):953–973. https://doi.org/10.1038/s41578-022-00464-7

Authors and Affiliations

Weiqin Sheng[1] · Ying Li[2] · Chunlian Qin[3] · Zhonghai Zhang[1] · Yuxiang Pan[3] · Zhicheng Tong[4] · Chong Teng[4] · Xinwei Wei[5]

✉ Weiqin Sheng
shengwq@hdu.edu.cn

✉ Ying Li
yingli@zcmu.edu.cn

✉ Chong Teng
tengchong1984@zju.edu.cn

✉ Xinwei Wei
weixinwei@zju.edu.cn

[1] School of Electronic Information, Hangzhou Dianzi University, Hangzhou 310018, China

[2] College of Basic Medical Sciences, Zhejiang Chinese Medical University, Hangzhou 310058, China

[3] ZJU-Hangzhou Global Scientific and Technological Innovation Center, Zhejiang University, Hangzhou 311200, China

[4] Department of Orthopedics, The Fourth Affiliated Hospital, Zhejiang University School of Medicine, Yiwu 322000, China

[5] Key Laboratory of Advanced Drug Delivery Systems of Zhejiang Province, College of Pharmaceutical Sciences, Zhejiang University, Hangzhou 310058, China